

Bayesian Image Analysis in Fourier Space

John Kornak¹, Karl Young², and Eric Friedman³

¹University of California, San Francisco, USA

²University of California, San Francisco, USA (Retired)

³International Computer Science Institute, Berkeley, USA

June 1, 2023

Abstract

Bayesian image analysis has played a large role over the last 40+ years in solving problems in image noise-reduction, de-blurring, feature enhancement, and object detection. However, these problems can be complex and lead to computational difficulties, due to the modeled interdependence between spatial locations. The Bayesian image analysis in Fourier space (BIFS) approach proposed here reformulates the conventional Bayesian image analysis paradigm as a large set of independent (but heterogeneous) processes over Fourier space. The original high-dimensional estimation problem in image space is thereby broken down into (trivially parallelizable) independent one-dimensional problems in Fourier space. The BIFS approach leads to easy model specification with fast and direct computation, a wide range of possible prior characteristics, easy modeling of isotropy into the prior, and models that are effectively invariant to changes in image resolution.

Keywords: Bayesian image analysis, Fourier space, Image priors, k-space, Markov random fields, Statistical image analysis.

1 Introduction

Bayesian image analysis models provide a solution for improving image quality in image reconstruction/enhancement problems by incorporating *a priori* expectations of image characteristics along with a model for image noise, i.e., for the image degradation process (Winkler, 1995; Guyon, 1995; Li, 2009). However, conventional Bayesian image analysis models, defined in the space of conventional images (hereafter referred to as “image space”) can be limited in practice because they can be difficult to specify and implement (requiring problem-specific code) and they can be slow to compute estimates for. Furthermore, Markov random field (MRF) model priors in conventional Bayesian image analysis (as commonly used for the type of problem discussed here) are not invariant to changes in image resolution (i.e., model parameters and MRF neighborhood size need to change when pixel dimensions change in order to retain the same spatial characteristics; this can be a problem when images are collected across multiple sites with different acquisition parameters or hardware) and are difficult to specify with isotropic autocovariance (i.e., with direction-invariant covariance).

Our approach to overcoming the difficulties and limitations of the conventional Bayesian image analysis paradigm, is to move the problem to the Fourier domain and reformulate in terms of spatial frequencies: *Bayesian image analysis in Fourier space* (BIFS). Spatially correlated prior distributions (priors) that are difficult to model and compute in conventional image space, can be successfully modeled via a set of independent priors across locations in Fourier space.

A prior is specified for the signal at each Fourier space location (i.e. at each spatial frequency) and *Parameter functions* are specified to define the values of the parameters in the prior distribution across Fourier space locations, i.e. we specify probability density functions (pdfs) over Fourier space that are conditionally independent given known values of parameter functions. The original high-dimensional problem in image space is thereby broken down into a set of one-dimensional problems, leading to easier specification

and implementation, and faster computation that is further trivially parallelizable. The fast computation coupled with trivial parallelization has the potential to open up Bayesian image analysis to big data imaging problems. Furthermore, the BIFS approach carries with it numerous useful properties, including easy specification of isotropy and consistency in priors across differing image resolutions for the same field of view.

Note that the BIFS approach is distinct from shrinkage prior methods that have been used previously in Fourier, wavelet or other basis set prior specifications (e.g. Olshausen (1996); Levin and Weiss (2007)). BIFS does not seek to smooth by generating a sparse representation in the transformed space through simple thresholding with the hope that it provides *a priori* desired spatial characteristics. Rather, the goal of BIFS is to fully specify the prior distribution over Fourier space in the same spirit as Markov random field or other spatial priors as specified in Bayesian image analysis, i.e., to fully represent as faithfully as possible *a priori* expected characteristics of the true/optimal image.

1.1 Bayesian image analysis

The general image analysis problem can be described as follows: Consider observed image data, y , that have been degraded by some "noise" process. The goal is to get an optimal estimate of the undegraded (and generally unobserved) version of the image (x); this process of estimating the undegraded image will be referred to as *reconstruction*. The objective of the Bayesian image analysis approach is to attempt to optimally reconstruct x based on observing y given knowledge of the image noise/degradation process and prior knowledge about properties that x should have. The optimization being performed with respect to minimizing some loss function of the posterior. Sometimes, interest may lie not in reconstructing the true image itself, but in generating a version of the image that may enhance certain features or properties (e.g. in cancer detection it would be useful to enhance tumors in an image to make it easier for the radiologist to detect and delineate them). In this case, the optimal x that we wish to construct will be an enhanced version of the true (undegraded) image with the prior designed to emphasize desirable characteristics of an enhanced image.

1.2 Conventional Bayesian image analysis:

Consider x to be a true or idealized image (e.g., noise-free or with enhanced features) that we wish to recover from a sub-optimal image dataset y . (Note that we are using the common shorthand notation of not explicitly distinguishing the random variables and the corresponding image realizations (Besag, 1989; Besag et al., 1991), i.e., we use lower case x and y .) The Bayesian image analysis paradigm incorporates *a priori* desired spatial characteristics of the reconstructed image via a prior distribution ("the prior") for the "true" image x : $\pi(x)$; and the noise degradation process via the likelihood: $\pi(y|x)$. The prior and likelihood are combined via Bayes' Theorem to give the posterior: $\pi(x|y) \propto \pi(y|x)\pi(x)$ from which an estimate of x can be extracted, e.g., the ubiquitous *maximum a posteriori* (MAP) solution obtained by determining the image associated with the mode of the joint posterior distribution.

1.2.1 Markov random field (MRF) priors:

The most common choice for the prior in conventional Bayesian image analysis is a Markov random field (MRF) model (Besag, 1974; Geman and Geman, 1984; Besag, 1986, 1989; Besag et al., 1991; Winkler, 1995; Guyon, 1995; Li, 2009; Swain et al., 2013; Sonka et al., 2014). MRF priors are used for imposing expected *contextual information* to an image such as spatial smoothness, textural information (small-scale pattern repetition), edge configurations (patterns of locations of boundaries with large intensity differences) etc. MRF methods provide improvement over deterministic filtering methods by *probabilistically* interacting with the data to smooth, clean, or enhance images, by appropriately weighting information from the data (via the likelihood) with the MRF prior to form the posterior probability distribution (the posterior) (Besag et al., 1991).

The definition of an MRF over a set of locations S is given via a conditional specification of each pixel (or voxel in 3D) intensity x_s at location s , given the set of neighboring pixels ∂s ; where "neighboring pixels" are defined in terms of being close to each other in space. Specifically, $\pi(x_s|x_{-\partial s}) = \pi(x_s|x_{\partial s})$, i.e. if the neighboring pixel values are known then remaining pixels add no further knowledge about the conditional

distribution of the intensity at s . The *full conditional posterior* for x_s given the data y and the values of x at all sites other than s , denoted by x_{-s} , can therefore be written as

$$\pi(x_s|y, x_{-s}) \propto \pi(y_s|x_s)\pi(x_s|x_{\partial s}), \quad (1)$$

(making the common assumption that the noise degradation process is independent across pixels). Note that the full conditional posterior at a pixel depends on its set of neighbors (even if that neighborhood is small) and therefore the joint distribution over all pixels is highly interdependent (the covariance matrix will generally be dense). Note also that the Hammersley-Clifford Theorem (Besag, 1974) allows an alternate (and equivalent) joint specification of MRFs in terms of the product of Gibbs measures over cliques (sets of inter-connected neighbors); these include the highly used set of intrinsic pairwise difference priors (Besag, 1989). However, the difficulties of dealing with a highly inter-dependent process remain.

1.2.2 Other conventional Bayesian image analysis priors

Other “higher level” Bayesian image analysis models exist that use priors to describe characteristics of objects in images through their geometrical specification (Grenander, 1993; Baddeley and van Lieshout, 1993; Rue and Hurn, 1999; Grenander et al., 2000; Ritter and Gallegos, 2002; Sheikh and Shah, 2005). However, these models have been used less frequently than MRF-based models, most likely because they often need highly problem-specific computational approaches, and are more difficult to specify, implement and compute.

1.3 Basis set representation methods for image analysis

There is considerable literature on methods for representing processes in terms of basis set representations, see e.g., the field of functional analysis (Ramsay and Silverman, 2005, 2002; Morris, 2014). Both Fourier and wavelet space basis sets can be used for functional analysis (including approaches with a Bayesian emphasis) (Chipman et al., 1997; Abramovich et al., 1998; Leporini and Pesquet, 2001; Johnstone and Silverman, 2005; Ray and Mallick, 2006; Nadarajah and Kotz, 2007; Christmas, 2014). However, these basis function approaches have mostly focused on using either simple priors based on L1/L2 regularization functions, and/or coefficient thresholding in the transformed space of the basis set; the aim being to shrink or get rid of the majority of coefficients.

Fourier/wavelet basis set shrinkage/thresholding based methods have seen multiple applications to the field of image analysis (including from a Bayesian perspective through L1/L2 regularization). In particular, methods for image processing have been developed using Fourier, wavelet and other bases sets (Olshausen, 1996; Donoho and Huo, 1999; Buccigrossi and Simoncelli, 1999; Figueiredo and Nowak, 1999; Donoho and Huo, 2002; Chang et al., 2000; Portilla et al., 2003; Candès and Donoho, 2004; Levin et al., 2007; Levin and Weiss, 2007; Pavlicová et al., 2008; Vijay et al., 2012; Li and Ghosal, 2014). By using an appropriate basis set, the sparse representation in that space is expected to generate processed images with certain characteristics. For example, sparse Fourier or wavelet representations can lead to noise reduction back in image space. (The intuition here is that removed coefficients with a small contribution to the overall signal are considered to be more likely dominated by noise.) However, in contrast to the Bayesian image analysis in the Fourier space approach that we develop here, there is no explicit *a priori* model for expected structure in the true image, other than that the true image might be well represented by a small subset of the basis functions. The BIFS paradigm provides a comprehensive approach to characterizing image priors by modeling specific priors at all Fourier space locations.

Fourier representations of Gaussian Markov random fields (GMRFs) have been used in order to generate fast simulations when the GMRF neighborhood structure can be represented by a block-circulant matrix, i.e. such that the GMRF can be considered as wrapped on a 2D torus: see Ch. 2.6 of Rue and Held (2005). We will explore the relationship between this Fourier space representation and a special case of the Bayesian image analysis in Fourier space approach we are proposing in Section 4.1.

Finally, there are a couple of interesting Fourier space-based Bayesian image analysis approaches that are of interest. Baskaran and Millane (1999) define a prior for the modulus (alternatively referred to as the magnitude) of the signal in Fourier space to infer the signal. It is motivated by a specific problem in X-ray crystallography where only the modulus of the Fourier transform can be measured, but not the argument (often referred to as the phase by physicists and engineers), and uses prior information over a

known part of the signal which is spherically symmetric. Staib and Duncan (1992) use a different idea of generating deformable models for finding the boundaries of 2D objects in images based on elliptic Fourier decompositions.

1.4 The Bayesian Image analysis in Fourier space approach

In this paper, we define a complete framework for specifying a wide range of spatial priors for continuous-valued images as models in Fourier space. The methodological benefit of working with Bayesian image analysis in Fourier space (BIFS) is that it provides the ability to model a range of stationary spatially correlated processes in conventional image space as independent processes across spatial frequencies in Fourier space.

The range of advantages afforded by transforming the Bayesian image analysis problem into Fourier space include:

- a) *easy model specification*: expected spatial characteristics in images are modeled as *a priori* expectations of the contribution of spatial frequencies to the BIFS reconstruction (e.g. smooth reconstructions require higher signal at lower spatial frequencies).
- b) *fast and easy computation*: specifying independence over Fourier space through BIFS means that optimization is based on a large set of low-dimensional problem (as opposed to a single high-dimensional problem).
- c) *modular structure*: allows for relatively straightforward changes in prior model.
- d) *resolution invariance in model specification*: BIFS allows for simple, generic specification of the prior, independent of image resolution.
- e) *straightforward specification of isotropic models*: BIFS allows for consistent specification of the prior in different directions, even when pixel (or voxel) dimensions are not isotropic.
- f) *ability to determine fast (and if desired, spatially isotropic) approximations to Bayesian MRF priors*: BIFS priors can be generated to mimic the behavior of many traditional prior models, providing users experienced with using MRFs with fast (non-iterative) counter-parts that can be implemented via BIFS representations.

2 BIFS Modeling Framework

Consider x to be the true (or idealized/enhanced) image that we wish to recover from a degraded or sub-optimal image dataset y . Instead of the conventional Bayesian image analysis approach of generating prior and likelihood models for the true image x based on image data y directly in terms of pixel values, we formulate the models via their discrete Fourier transform representations: $\mathcal{F}x$ and $\mathcal{F}y$. Using Bayes' Theorem, the posterior, $\pi(\mathcal{F}x|\mathcal{F}y)$, is then,

$$\pi(\mathcal{F}x|\mathcal{F}y) \propto \pi(\mathcal{F}y|\mathcal{F}x)\pi(\mathcal{F}x) . \tag{2}$$

The key aspect of the BIFS formulation that leads to its useful properties of easy specification and computational speed, is that we specify both the prior and likelihood (and therefore the posterior) to consist of a set of independent processes over Fourier space locations. In order to induce spatial correlation in image space, the parameters of the prior distributions are specified so as to change in a systematic fashion over Fourier space; independent (but heterogeneous) processes in Fourier space are thereby transformed into spatially correlated processes in image space (Zeger, 1985; Lange and Zeger, 1997; Peligrad and Utev, 2006). Heuristically, the realized signal at each position in Fourier space corresponds to a spatially correlated process in image space (at one particular spatial frequency). In general therefore, linear combinations of these spatially correlated signals (such as that given by the discrete Fourier transform) will also lead to a correlated process in image space. This independence-based specification over Fourier space can be contrasted with the conventional Bayesian image analysis approach of using Markov random field (MRF) priors for imposing spatial correlation properties, where the Markovian neighborhood structures are used to induce correlation

patterns across pixels via joint or conditional distributional specifications (Besag, 1974; Geman and Geman, 1984; Besag, 1989). In fact, as we discuss in Section 4.1 in certain instances MRF models exactly correspond to uncorrelated processes in Fourier space.

When specifying a spatially correlated prior in image space via a set of independent processes across Fourier space, the full conditional posterior at a Fourier space location $k = (k_x, k_y) \in [-\pi, \pi]^2$, or for volumetric data $(k_x, k_y, k_z) \in [-\pi, \pi]^3$, now only depends on the prior and likelihood at that same Fourier space location k , i.e.,

$$\pi(\mathcal{F}x_k | \mathcal{F}y) = \pi(\mathcal{F}x | \mathcal{F}y_k) \propto \pi(\mathcal{F}y_k | \mathcal{F}x_k) \pi(\mathcal{F}x_k) , \quad (3)$$

where we use $\mathcal{F}x_k$ as shorthand for $(\mathcal{F}x)_k$. The joint posterior density for the image is then

$$\pi(\mathcal{F}x | \mathcal{F}y) \propto \prod_{k \in K} \pi(\mathcal{F}y_k | \mathcal{F}x_k) \pi(\mathcal{F}x_k) , \quad (4)$$

where K is the set of all Fourier space point locations in the (discrete) Fourier transformed image. Note that for our purposes we index Fourier space along direction $v \in \{x, y, z\}$ by $\{-N_v/2, \dots, 0, 1, \dots, N_v/2 - 1\}$, rather than the common alternative of $\{0, \dots, N_v - 1\}$, as it leads to a more convenient formulation for specifying BIFS prior models, i.e. such that they are centered at the zero frequency position of Fourier space. Furthermore, in order to account for the fact that (most) images are in practice real-valued, the Fourier transform must be conjugate (Hermitian) symmetric on the plane (or volume if 3D). A real-valued image output is ensured by considering a realization of the posterior distribution to be determined by the half-plane (half volume), the other half being conjugate symmetric to the first (see Liang and Lauterbur (2000), pp. 31 and 322). Therefore, for real-valued images, the BIFS posterior is only evaluated over half of Fourier space (and points on the line $x = 0$ if taking half-plane in the y -direction or conversely $y = 0$ for half-plane in the x -direction) and the remainder is obtained by conjugate reflection.

In defining priors as a process over Fourier space we are restricting the space of possible priors to generally stationary processes, similar to MRFs with neighborhood structure wrapped on the torus. (The ‘‘generally’’ qualifier is because of the very specific exception that the BIFS priors can be specified as non-stationary with respect to identification of the overall mean by placing an improper uniform prior at k -space point $(0, 0)$ for the modulus, i.e., leading to models with the same property as the intrinsic pairwise MRF priors. In practice, for image analysis problems where the goal is to enhance features, this restriction to stationarity is minimal except toward the edges of an image; and the effects at the edges can be mitigated by expanding the field of view of the data (e.g. by setting pixel values in the expanded edges to the overall image mean or to an expanded neighborhood mean). Furthermore, in many medical imaging applications the area of interest is far from the edges of the field of view and much of the boundary corresponds to regions outside of the body and therefore the intensity levels are flat toward the edges.

2.1 The BIFS prior

A two-step process is used to specify the BIFS prior distribution over Fourier space. First, the distributional form of the prior for the signal intensity at each Fourier space location is specified, i.e., $\pi(\mathcal{F}x_k)$. Second, the parameters of each of the priors are specified at each Fourier space location using *parameter functions*. In order to specify the parameter values across all Fourier space locations simultaneously, we specify a parameter function over Fourier space that identifies the value of each parameter at each Fourier space location. Specifically, for some parameter α_k of $\pi(\mathcal{F}x_k)$ we choose the parameter function f_α such that the $\alpha_k = f_\alpha(k)$. For most problems in practice it is desirable to choose a spatially isotropic prior, which can be induced by specifying $\alpha_k = f_\alpha(|k|)$, where $|k| = \sqrt{k_x^2 + k_y^2}$ in 2D or $\sqrt{k_x^2 + k_y^2 + k_z^2}$ in 3D, i.e., such that f only depends on the distance from the origin of Fourier space. In the remainder of this paper, description is given in terms of 2D analysis, but notational extension and application to 3D volumetric imaging is straightforward.

2.2 The Parameter Functions:

In order to control spatial characteristics of the prior and likelihood we develop the concept of a *parameter function*. The parameters of the independent priors over Fourier space are specified according to parameter

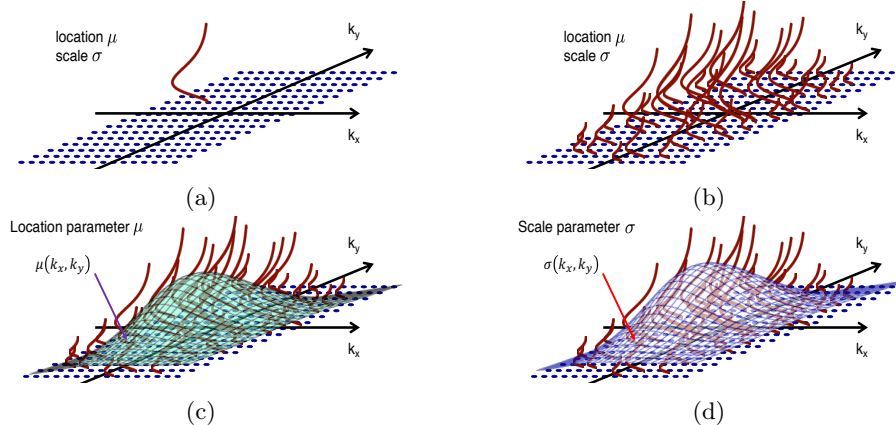


Figure 1: Schematic of parameter function set up for the signal modulus of the signal where the distribution at each Fourier space location requires specification of a location parameter, μ , and scale parameter, σ . Panel (a) gives the layout of Fourier space with a pdf at a single Fourier space location. Panel (b) extends to show pdfs at multiple location, each of which has a location and scale parameter as described by the parameter functions for location shown as a surface in Panel (c). Panel (d) gives the parameter function for the scale parameter which is here assumed to be proportional to the location parameter for the Modulus, i.e. $\mu(k_x, k_y) = c\sigma(k_x, k_y)$; where c is a positive constant. This can be a practical, but not necessary assumption.

functions that describe the pattern of parameter values over Fourier space (see illustrations of Figure 1); the parameter function traces out the values of parameters for the prior over Fourier space. In general, the parameter function is multivariate, with one dimension for each parameter of the prior distribution used at each Fourier space location, e.g. Figure 1 illustrates parameter functions for distributions with two parameters (scale and location). Note that for some models it proves more convenient to specify parameter functions for transformations of the original distribution parameters; e.g. for the gamma distribution the parameter functions might be defined for the mean and variance which can then be transformed to the shape and scale (or rate) parameters.

Separate and independent priors, and associated parameter functions, are specified for each of the modulus and argument of the complex value at each Fourier space location. Working with the modulus and argument provides a more convenient framework for incorporating prior information at specific Fourier space locations (i.e., specific spatial frequencies) than working with the real and imaginary components. The convenience arises because prior information (e.g., expected characteristics of smoothness, edges, or features of interest) can be directly specified via the modulus of the process, with the argument being treated independently of the modulus. However, real and imaginary components are more difficult to specify since signal can shift between them through the translation of objects in the corresponding image space; for example, a rigid movement of an object in an otherwise constant intensity image will cause shifts between real and imaginary components (by the Fourier transform shift Theorem) whereas in the modulus/argument specification it will only change the argument of the signal.

2.3 Priors and parameter functions for signal modulus

Modulus prior form:

Any continuous distribution can be used to represent the prior at each point in Fourier space. It is also possible to allow the distribution itself to differ in different regions of Fourier space, though we do not pursue that here except to allow for a different distributional form at the $k = (k_x, k_y) = (0, 0)$ spatial frequency (corresponding to the mean intensity). However, there is an advantage to specifying priors that only have mass for non-negative real numbers; if priors are chosen that can take negative values then a switch from positive to negative corresponds to a π discontinuous change in the argument which would typically lead to an overall representation of prior beliefs that is unrealistic. In practice, we find that the choice for the form

of the parameter function (discussed below) has a larger influence on the spatial characteristics of the prior than the choice of prior distribution model. For the purpose of computational expedience it therefore often make sense to choose conjugate priors to the likelihood for the modulus when available. For example, we could use a Gaussian (normal) prior for the location parameter of a lognormal likelihood with known scale parameter for the noise process; specification of noise parameters will be discussed in Section 2.7.

Modulus parameter function forms:

The parameter functions for the modulus are specified as a set of 2D functions over Fourier space (in terms of k_x and k_y): often one for each of location (e.g. mean) and scale (e.g. standard deviation, sd), or/and any other parameters of the prior. The center of Fourier space, i.e., the $k = (k_x, k_y) = (0, 0)$ frequency, is the prior for the overall image intensity mean. At this location, it is reasonable to choose a different pdf than at all other locations. Indeed, the prior at $k = (k_x, k_y) = (0, 0)$ can be modeled as improper, e.g. uniform on the real line, leading to an intrinsic, non-stationary prior for the image (Künsch, 1987; Besag et al., 1991).

In general, useful priors across Fourier space are generated by allowing the parameter function for the location parameter to decrease with increasing distance from the center of Fourier space. In our experience, the functional form of the descent has a major impact on the properties of the prior model; much more so than the form of the pdf chosen for each Fourier space location. In addition, specific ranges of frequencies can be accentuated by increasing the parameter function for the location parameter over those frequencies, leading to enhanced spatial frequency bands as a function of distance from the origin.

When considering how to define the modulus parameter function for the scale parameter, we find that setting it to be proportional to that for the mean is often a good strategy though the method allows for different strategies wherever warranted.

Other parameter functions (i.e. parameter functions that do not represent location or scale) may be intuitively more difficult to specify. We do not consider any such functions here, as we find priors with one or two parameters at each Fourier space location to be satisfactory for problems we have encountered.

One situation where a parameter function for something other than the location and scale parameters might be useful would be when mixture distribution priors are appropriate. In particular, a mixture of two distributions could be considered where one of the distributions consists of a probability mass specified at zero. The variation in probability mass for zero at each Fourier space location can itself be specified by a parameter function. For example, one might want to specify increased probability of exact zeros the further away a point is from the origin of Fourier space. Such a prior/parameter function combination would have the effect of encouraging more sparsity at Fourier space locations further from the origin. If high enough mass were specified for zeros across Fourier space this could lead to sparsely represented reconstructions that could in turn be useful when storage space is an issue. The end result would provide lasso style shrinkage in combination with prior information about spatial properties.

2.4 Priors and parameter functions for signal argument

Generally, we have limited prior knowledge about the argument of the signal; the argument is related to the relative positioning of objects in the image; moving (shifting) objects around in an image will change the argument of related frequencies. We therefore specify the prior for the argument to reflect *a priori* ignorance by using an *i.i.d.* uniform distribution on the circle at all Fourier space locations, i.e., we define flat parameter functions representing $-\pi$ and π as the parameters for $U(a, b)$ distributed arguments at all Fourier space locations. A notable exception to using uniform priors for the argument occurs when the prior is being built empirically from a database of images; we discuss this scenario in our final (simulation) example of Section 5.1.

2.5 BIFS likelihood

Similar to the prior, the BIFS likelihood is modeled separately for the modulus and argument of the signal at each Fourier space location. Because we model based on independence across Fourier space points, a range of different noise structures (specified in Fourier space) can readily be incorporated into the likelihood $\pi(\mathcal{F}y_k | \mathcal{F}x_k)$.

The parameter(s) of the likelihood needs to be provided or estimated for the BIFS algorithm. A straightforward approach to this estimation is to extrapolate any areas of the original image that are known to consist only of noise to an image of equal size to the original image, and then Fourier transform to estimate the corresponding noise distribution in Fourier space.

In practice, not knowing the noise standard deviation is not a major impediment to proceeding with Bayesian image analysis. The noise in the image and the precision in the prior trade off with one another in the Bayesian paradigm and therefore the parameter functions of the prior can be adjusted to produce a desired effect *a posteriori*. This *ad hoc* approach is common to much Markov random field prior modeling in Bayesian image analysis; the appropriate setting of hyper-parameter values is a difficult problem in general and often they are left as parameters to be tuned by the user (Sørbye and Rue, 2014).

2.6 Posterior estimation

Posterior estimation in conventional Bayesian image analysis tends to focus on MAP estimation (i.e., minimizing a 0 – 1 loss function) primarily because it is usually the most computationally tractable. In the BIFS formulation the MAP estimate can be efficiently obtained by independently maximizing the posterior distribution at each Fourier space location, i.e, $x_{\text{MAP}} = \mathcal{F}^{-1}(\mathcal{F}x_{\text{MAP}})$ where $\mathcal{F}x_{\text{MAP}} = \{\mathcal{F}x_{k,\text{MAP}}, k = 1, \dots, K\}$ and $\mathcal{F}x_{k,\text{MAP}} = \max_{\mathcal{F}x_k} \{\pi(\mathcal{F}x_k|\mathcal{F}y)\} = \max_{\mathcal{F}x_k} \{\pi(\mathcal{F}x_k|\mathcal{F}y_k)\}$. This contrasts with conventional Bayesian image analysis, where even the most computationally convenient MAP estimates typically require iterative computation methods such as conjugate gradients or expectation-maximization. Beyond the MAP estimate, it is straightforward to simulate from the posterior of BIFS models to get mean estimates such as minimum mean squares estimate (MMSE) estimates (Winkler, 1995) or other summaries of samples from the posterior. The independence of posterior distributions over Fourier space implies that simple Monte Carlo simulation is all that is required to obtain posterior samples. This is in contrast to conventional Bayesian image analysis, where some form of Markov chain Monte Carlo (MCMC) simulation is typically needed: leading to issues of chain convergence and mixing that need to be dealt with (Gilks et al., 1996). The general computational approach to implementing BIFS follows that of Algorithm 1.

Note that, when an uninformative uniform prior is used for the argument, and the likelihood is symmetric about the observed argument in the data, the corresponding maximum of the posterior at that Fourier space point is simply the argument of the Fourier transformed data at that point. Therefore, under these conditions, the exact form of the likelihood is unimportant for the MAP estimate. This leads to added simplicity for obtaining the MAP image estimate and is particularly beneficial when working with Gaussian noise in image space where the corresponding distribution for the argument in Fourier space is difficult to work with given the lack of analytical solution (See Section 2.7).

Algorithm 1 General BIFS implementation

```

Fast Fourier transform (FFT) image data,  $y$ , into Fourier space,  $\mathcal{F}y$ 
Specify noise distribution/likelihood in Fourier space  $\pi(\mathcal{F}y_k|\mathcal{F}x_k)$ 
Specify prior distribution form  $\pi(\mathcal{F}x_k)$ 
Specify parameter functions for each of modulus and argument of the signal
for each  $k \in K$ , do
    Obtain  $\pi(\mathcal{F}x|\mathcal{F}y) \propto \pi(\mathcal{F}y|\mathcal{F}x)\pi(\mathcal{F}x)$ 
    Generate posterior estimates/summaries/simulations at each  $k$  via MAP or Monte Carlo
end for
Inverse FFT posterior estimates/summaries/simulations back to image space.

```

2.7 Modeling Gaussian *i.i.d.* noise in image space

A common model for the noise in images is to assume that the image intensities are contaminated by *i.i.d.* Gaussian noise. Although *i.i.d.* Gaussian noise in image space transforms to complex Gaussian noise in Fourier space with independent real and imaginary components, when the real and imaginary components are transformed to modulus and argument, the associated errors are not Gaussian distributed. The corresponding

likelihood model for the modulus is the Rician distribution which takes the following form (Rice, 1944, 1945; Gudbjartsson and Patz, 1995; Rowe and Logan, 2004; Miolane et al., 2017):

$$\pi(r|\rho, \sigma) = \frac{r}{\sigma^2} \exp\left(-\frac{r^2 + \rho^2}{2\sigma^2}\right) I_0\left(\frac{r\rho}{\sigma^2}\right); \quad r, \rho, \sigma \geq 0 \quad (5)$$

where $I_0(z)$ is the modified Bessel function of the first kind with order zero, σ is the standard deviation of the real and imaginary Gaussian noise components in Fourier space (*i.i.d.* real and imaginary parts), r is the observed modulus of the signal, i.e., $\text{Mod}(\mathcal{F}y_k)$ in the BIFS formulation, and ρ is the noise-free modulus, $\text{Mod}(\mathcal{F}x_k)$.

Note that in the Rician likelihood, the standard deviation of each of the real and imaginary components is the σ parameter of the Rician distribution. Therefore, by obtaining an estimate of the noise level in image space, the σ parameter over Fourier space can itself be estimated by dividing the estimated standard deviation of the noise in image space by 4.

The corresponding likelihood for the argument takes the form (Gudbjartsson and Patz, 1995; Rowe and Logan, 2004):

$$\pi(\psi|\rho, \theta, \sigma) = \frac{\exp\left(-\frac{\rho^2}{2\sigma^2}\right)}{2\pi} \left[1 + \frac{\rho}{\sigma} \cos(\psi - \theta) \exp\left(\frac{\rho^2 \cos^2(\psi - \theta)}{2\sigma^2}\right) \int_{r=-\infty}^{\frac{\rho \cos(\psi - \theta)}{\sigma}} \exp\left(-\frac{z^2}{2}\right) dz \right] \quad (6)$$

where $\psi \in [-\pi, \pi)$ is the observed argument of the signal, $\text{Arg}(\mathcal{F}y_k)$, and $\theta \in [-\pi, \pi)$ is the noise-free argument, $\text{Arg}(\mathcal{F}x_k)$.

Posterior estimation for *i.i.d.* Gaussian noise in image space

Modulus MAP estimate: If one is interested in the MAP image estimate (i.e. the image associated with minimizing the 0 – 1 loss function of the posterior) then the mode of the posterior for the modulus at each Fourier space location needs to be estimated. A first approach might be to consider a direct off-the-shelf optimization, but we have found this to be problematic. The problem is that this is a non-trivial optimization (at least in the Rician case) because at many Fourier space locations the prior and likelihood can be highly discordant, i.e. the modes of the prior and the likelihood can be very far apart with very little density in between for both distributions. This discordance is not entirely surprising and exists for the same reason that typical conventional image analysis priors are not full representations of prior beliefs for an image, but instead typically only represent expected local characteristics such as smoothness of the image (Besag, 1993; Green, 1990). In practice, we experience direct numerical optimization to break down in extremely discordant cases.

We therefore propose the following approach to MAP estimation with the Rician likelihood (we drop the k subscript for location in Fourier space to aid clarity). Take the Rician likelihood given in Equation (5) and multiply it by the prior for the modulus $\pi(\rho)$. The posterior is $\pi(\rho|r, \sigma) \propto \pi(r|\rho, \sigma)\pi(\rho)$ and we can take logs to simplify, drop constant terms, and find the maximum. Finally, take the second derivative to check that it is concave by bounding the derivative of the Bessel function.

For example, if we assume an exponential prior for ρ i.e. $\pi(\rho) \propto \exp\left(-\frac{\rho}{m}\right)$, take logs and simplify we get

$$\log \pi(\rho|r, \sigma) = c + \log\left(\frac{r}{\sigma^2}\right) - \frac{r^2 + \rho^2}{2\sigma^2} + \log\left[I_0\left(\frac{r\rho}{\sigma^2}\right)\right] - \frac{\rho}{m}$$

where c is a constant term. Now differentiate w.r.t. ρ and set to 0

$$-\frac{\rho}{\sigma^2} - \frac{1}{m} + \frac{r I_1\left(\frac{r\rho}{\sigma^2}\right)}{\sigma^2 I_0\left(\frac{r\rho}{\sigma^2}\right)} = 0$$

where $I_0(z)$ is the modified Bessel function of the first kind with order one, and define

$$b(\rho) = \frac{I_1\left(\frac{r\rho}{\sigma^2}\right)}{I_0\left(\frac{r\rho}{\sigma^2}\right)}$$

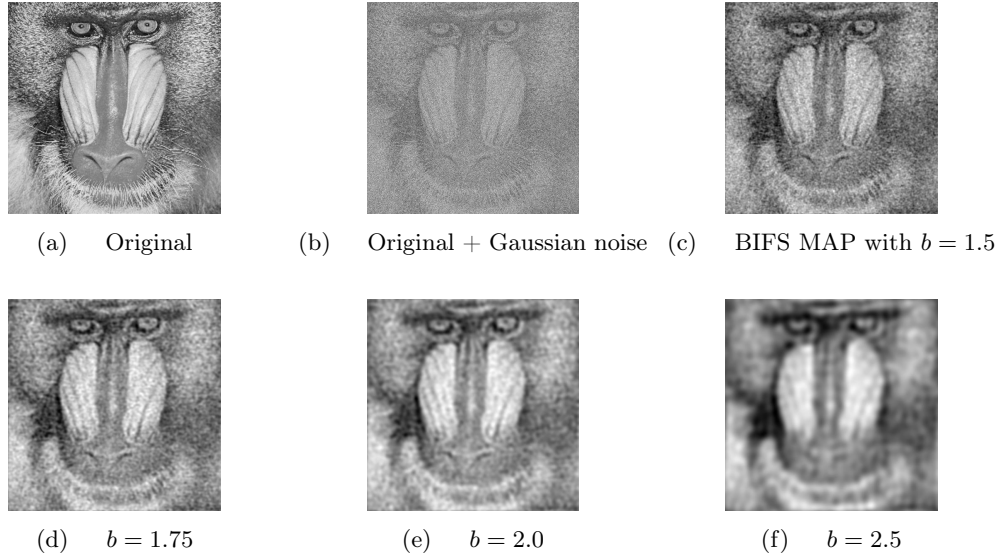


Figure 2: Mandrill pics, (a) original image; (b) Gaussian noise degraded image; (c) BIFS MAP with $b = 1.5$; (d) $b = 1.75$; (e) $b = 2$; (f) $b = 2.5$.

to get

$$\rho = rb(\rho) - \frac{\sigma^2}{m} \quad (7)$$

The posterior estimate of ρ can then be estimated quickly through iteration. Start with $\rho_0 = r$ and then iterate Equation 7 repeatedly as $\rho_{n+1} = rb(\rho_n) - \frac{\sigma^2}{m}$ to compute the MAP estimate of ρ . In practice this requires only a few iterations to get high accuracy. Note that the unconstrained maximum of the function may occur at negative values of ρ . In that case the posterior maximum for ρ is set to 0 because the function is monotonically decreasing to the right of the maximum. A similar iterative approach can be applied when considering other prior distributions for ρ .

Argument MAP estimate: Note that for a noise process with a uniformly random argument on the circle (as for *i.i.d.* noise in real and imaginary components), the likelihood at a Fourier space point has highest density at the argument of the data at that Fourier space location, i.e. $\text{Arg}(\mathcal{F}y_k)$. Therefore, since we adopt a uniform prior for the argument on the circle, then the argument corresponding to the maximum of the posterior is also $\text{Arg}(\mathcal{F}y_k)$. This property will always be true when using the uniform prior on the circle for the Argument provided the likelihood for the argument is symmetric about its maximum; this condition will be necessarily true for all noise processes with uniformly random argument.

2.8 Example 1 – Smoothing/denoising

Figure 2 shows the BIFS MAP reconstruction results of a grayscale test image of a Mandrill monkey face using the exponential prior, Rician likelihood, and a parameter function for the exponential distribution mean of the form $f_\mu(|k|; a, b) = a/|k|^b$ (inverse exponentiated distance) at all locations except for the origin, $k = (0, 0)$, where the prior was an improper uniform distribution on the real line. The top-left panel (a) shows the original noise-free image and the top-middle panel (b) shows the same image with added Gaussian noise (zero mean with SD \approx one third of the dynamic range of the original image). The noisy image in panel (b) is used as the input degraded image into the BIFS models. The remaining panels show BIFS MAP reconstructions for different values of b , namely (c) $b = 1.5$, (d) $b = 1.75$, (e) $b = 2$, and (f) $b = 2.5$. The parameter value for a was chosen based on matching the power of the parameter function (sum of square magnitude) to that in the observed data over all Fourier space points other than at $k = (0, 0)$. The image intensities in each panel are linearly re-scaled to use the full dynamic range. Re-scaling is appropriate in situations where image features are of interest, but not if quantification of intensities is of interest.

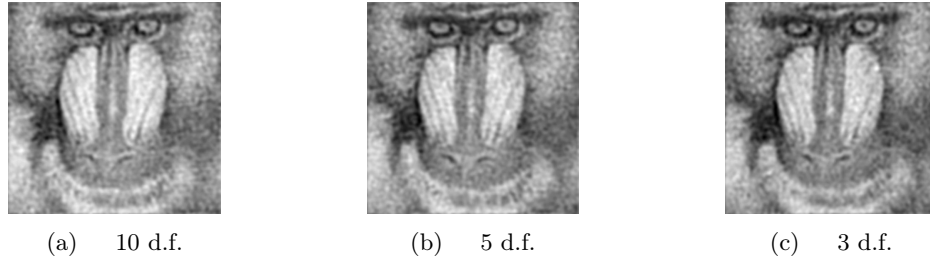


Figure 3: Mandrill pics reconstructed under wrong noise distribution (Student- t) all with $b = 2$, (a) 10 d.f.; (b) 5 d.f.; (c) 3 d.f.

In examining the MAP reconstructions of Panels (c) to (e) it is clear that the overall level of smoothness increases (and noise suppressed) as the value of b increases. This is to be expected since higher b implies faster decay of the parameter function for the signal modulus with increasing distance from the origin. However, as a price for higher noise suppression, finer level features are lost. For example, by the $b = 2.5$ the whiskers and even nostrils of the Mandrill are smoothed away.

Robustness to heavy-tailed noise: In order to examine whether the BIFS reconstructions were robust to noise distributions with heavier tails, the BIFS procedure was repeated for data with added noise generated from Student t -distributions controlled to have the same SD but with different degrees-of-freedom (d.f.). Figure 3 displays the results of the reconstructions using the same priors as above with $b = 2$ and with d.f. of (a) 10 d.f.; (b) 5 d.f.; and (c) 3 d.f. The reconstructions are visually quite similar to each other with slight differences only showing up with the very heavy-tailed 3 d.f. reconstruction. Results from other values of b were also similarly robust.

2.9 Example 2 – Frequency enhancement

The example in Figure 4 displays a range of BIFS reconstructions for a grayscale test image of a surface patch on the moon. The reconstructions are again focused on using an exponential prior with Rician likelihood for the parameter function of the signal modulus. Panel (a) shows the original image and Panel (b) shows the *i.i.d.* additive Gaussian noise degraded image serving as the image to apply reconstruction. Panel (c) displays the BIFS reconstruction based on applying the denoising prior parameter function used in Example 1 with $b = 2$. Panels (d) through (f) show frequency selective priors for which prior weight is only given to Fourier space locations within a specific range of distances from the origin (*frequency selective torus parameter function*); these priors are also smoothed by an isotropic Gaussian spatial kernel with SD of 1.5 Fourier space pixels in each of the k_x and k_y directions. For Panel (d) distances of 1 to 5 pixels from the origin are given non-zero mass; in Panel (e) 10.01 to 15 pixels; and Panel (f) 15.01 to 60 pixels. Panels (g) through (i) show corresponding reconstructions where the parameter function is a weighted average of the torus parameter function directly above and the denoising parameter function of panel (C); weighted at 90% torus and 10% denoising. In all of the examples, the level of each of the parameter functions is adjusted to approximately match total power to that observed in the image data.

It is clear that the different torus parameter functions are providing results as expected in terms of focusing in on specific frequency windows. However, when mixed with other parameter functions such as the denoising prior useful compromises between the parameter function forms can be achieved. The addition of the denoising component in Panels (g) through (i) softens the harsh restriction to the specific frequency ranges. For example, while in Panel (d) the reconstruction is highly blurry, the reconstruction of Panel (g) allows enough higher resolution information to make the image less obviously blurry to view while still enhancing low frequency features. For the high range of frequencies of Panel (f) it is clear that the addition of the denoising component in Panel (i) is critical to be able to even understand the context of the image. The effect of combining the high-frequency selective prior with the denoising prior is to enhance smaller features. In particular, notice that this prior is able to identify the small crater that is pointed to by the top arrow in Panel (i) which is missed by the other priors with less high frequency information. Notice also that even though it is observable in panel (f) it is not easily distinguishable as a different type of object than the white spot at the middle of the dip in the large crater at the bottom indicated by the bottom arrow.

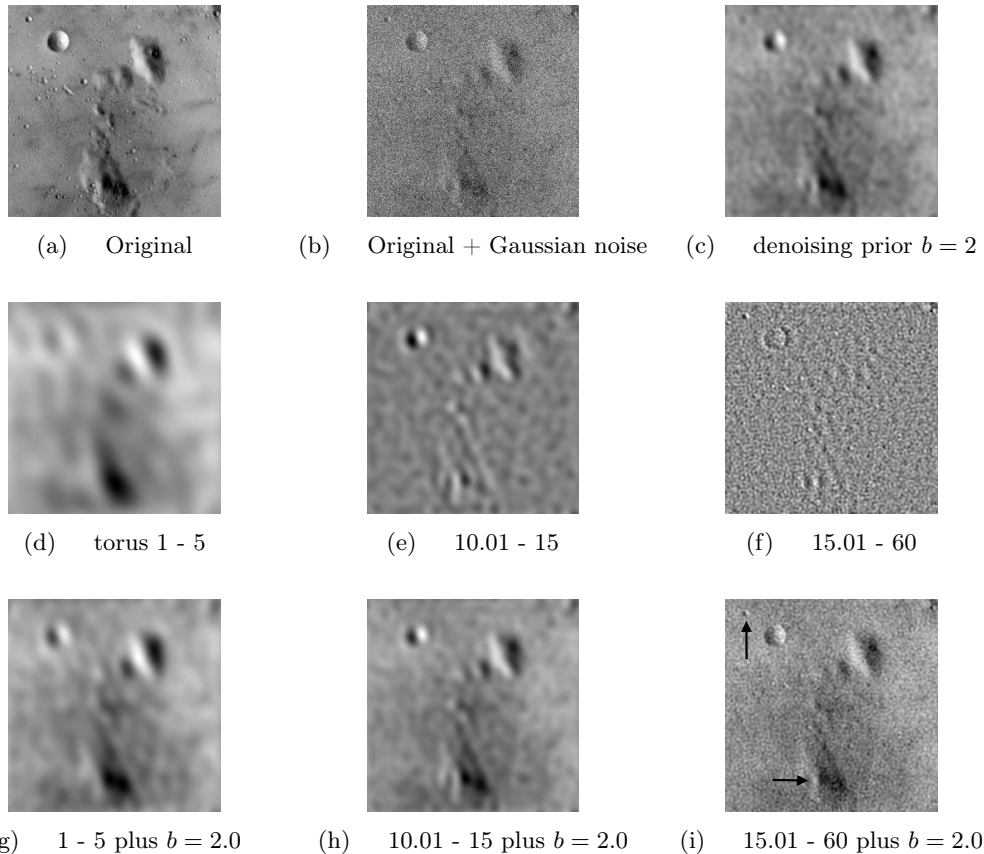


Figure 4: Moon pics, (a) original image; (b) Gaussian noise degraded image; (c) BIFS MAP estimate using denoising prior from Section 2.8 with $b = 2$; (d) BIFS MAP with "smoothed torus frequencies" based on distance ($|k|$) 1 - 5 from origin; (e) 10.01 - 15; (f) 15.01 - 30; (g) linear combination of smoothed torus 1 - 5 plus denoising prior from Section 2.8, i.e., the inverse exponentiated parameter function with $b = 2$; (h) 10.01 - 15 plus $b = 2$; (i) 15.01 - 60 plus $b = 2$.

Clearly, the design of these parameter functions is critical to the properties of the prior in a similar way to how the clique penalties of Markov random field priors operate. However, it is difficult to see how clique functions could be defined to produce priors with the properties of the frequency selective priors or their mixtures with denoising priors.

There is clearly considerable potential for designing parameter function / prior combinations for BIFS that can produce a range of image processing characteristics that are not readily achievable with MRF priors.

2.10 Example 3 – edge detection

The family of parameter functions described in the previous example can also prove useful for edge detection in images as illustrated in this example using a Gaussian noise contaminated version of the standard grayscale pirate test image. The sequence of images Figure 5 (d) to (f) shows how the removal of low frequency information isolates edge information. The upper limit on frequencies is chosen as a trade off between capturing the highest frequency edge information vs. potentially masking the edge information if there is too much high frequency noise, Figure 5 (g) to (i).

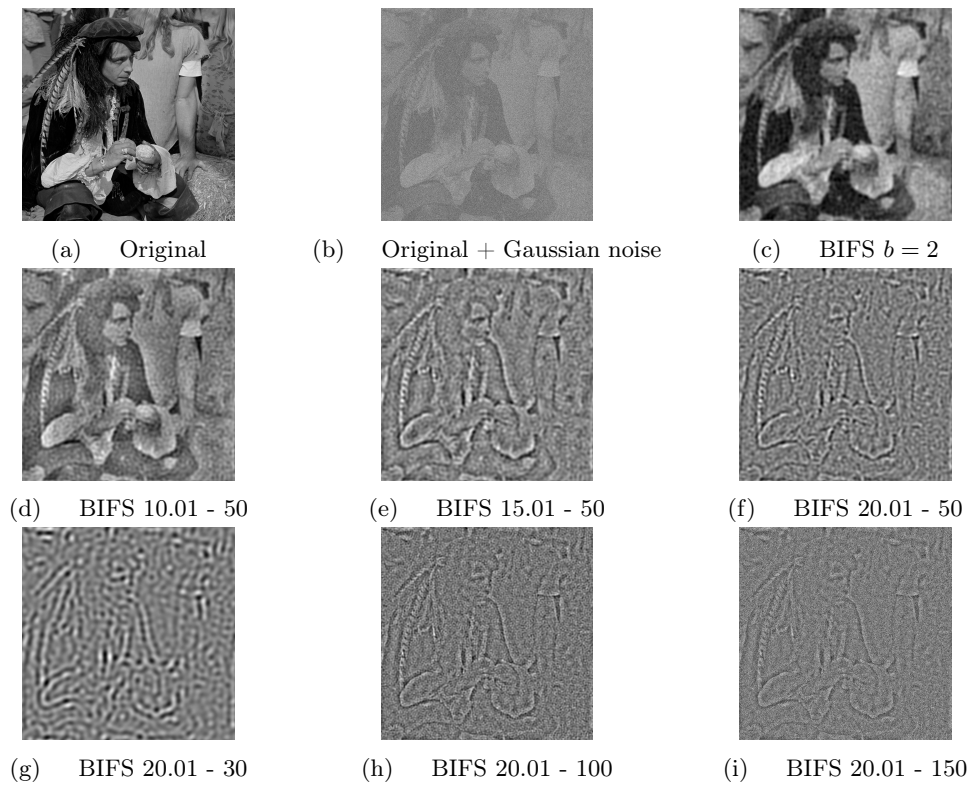


Figure 5: Pirate pics, (a) original image; (b) Gaussian noise degraded image; (c) BIFS denoising $b = 2$; (d) BIFS 10.01 - 50; (e) 15.01 - 50; (f) 20.01 - 60; (g) 20.01 - 30; (h) 20.01 - 100; (i) 20.01 - 200.

3 BIFS Properties

There are multiple properties of the BIFS formulation that prove advantageous relative to conventional MRF-priors and other Bayesian image analysis models:

3.1 Computational Speed:

The independence property of the BIFS formulation generally leads to improved computational efficiency over MRF-based or other conventional Bayesian image analysis models that incorporate spatial correlation structures into the priors in image space.

For MAP estimation, Bayesian image analysis using MRF priors requires high-dimensional iterative optimization algorithms such as iterated conditional modes (ICM) (Besag, 1989), conjugate gradients (Hestenes, 1969), or simulated annealing (Geman and Geman, 1984). Iterative processes are necessary when working in the space of the images because of the inter-dependence between pixels. In contrast, BIFS simply requires independent posterior mode estimation at each Fourier space location, and the inverse discrete Fourier transform of this set of Fourier space local posterior modes will provide the global posterior mode image. This independent-over-Fourier-space optimization approach also scales well with respect to increasing image size, increasing dimensionality (e.g. to 3D), or increasing prior model complexity. The level of computational complexity is basically $ng(k)$, where $g(k)$ is the complexity of the optimization at each Fourier space point. Therefore, for increased image size or dimension, the computation time is scaled by the proportional increase in the number of Fourier space points, whereas for increased complexity at each Fourier space point to $h(k)$ the total computation is simply scaled by $\frac{h(k)}{g(k)}$.

Computational improvements can similarly be obtained if one wishes to perform posterior mean or other estimation and credible interval generation. (Note that one has to be careful interpreting credible intervals for Bayesian image analysis models since the prior models are at best only rough approximations about characteristics of prior beliefs.) Markov random field prior models generally require high-dimensional Markov chain Monte Carlo (MCMC) posterior simulations to obtain the MMSE image estimate as the posterior mean. However, BIFS only requires at most low-dimensional MCMC to be performed at each Fourier space location. A single realization of the posterior parameter set from each Fourier space location can be inverse Fourier transformed to produce an independent realization of an image from the posterior distribution, thereby avoiding the difficulties of dealing with potentially slow mixing chains that often occur in Bayesian image analysis modeling when updating at the pixel-level.

In addition to the algorithmic speed up for MAP and MMSE estimation, the independence property of the Fourier space approach also allows for trivial parallelization because sampling for each Fourier space location can be performed independently. Therefore, acceleration of a factor close to the number of processors available can be achieved up to having as many processors as Fourier space points.

Finally, another aspect in which it is computationally more efficient to work in the BIFS framework comes about because it is much easier to try different prior models defined in Fourier space. In particular, one can very easily change the parameter functions for the prior, which in our experience has the biggest effect on the properties of the prior overall. Changing the form of the prior distribution at each Fourier space location takes more coding effort but is still much less work than writing code for different MRF-prior-based posterior reconstructions; trying different MRF priors (beyond simply changing parameter values) is typically a non-trivial task.

Overall, the computational speed afforded by BIFS, in addition to the potential for massive parallelization and flexibility of parameter functions, has great potential for the advancement of Bayesian image analysis and opens it up to play a larger role in Big Data imaging problems.

3.2 Resolution invariance

Specifying the prior in Fourier space leads to easy translation of the priors for changes in image resolution. When increasing resolution in image space by factors of two, the central region of the Fourier transform at higher resolution corresponds very closely to that of the complete Fourier transform at lower resolution; they correspond to the same spatial frequencies within the field of view. The lower resolution image is very close to a band-limited version of the image at higher resolution. Note that this is only approximate

as the increased resolution can slightly alter the magnitude of the measured Fourier components whose frequency is significantly lower than that of the resolution. However, this effect can be bounded by the ratio of the maximum resolution to that of the wavelength of the measured frequency so is typically quite small. This small change in magnitude will remain small in the posterior estimate when the parameter function is continuous.

When the resolution increases but not by a factor of two, the same approach of matching parameter functions over the frequency range can still be applied. However, there will no longer be a direct match of points over the lower frequencies and therefore there will be a less perfect match of the prior distributions overall.

The above described BIFS approach to matching over different resolutions contrasts with MRF models, for which in order to retain the spatial properties of the prior at lower frequencies, an increase in resolution would require careful manipulation of neighborhood structure and prior parameters to match spatial auto-covariance structures between the different resolution images (Rue and Tjelmeland, 2002).

3.3 Isotropy

In order to specify a *maximally isotropic* BIFS prior, all that is required is for the prior to be specified in such a way that the distribution at each Fourier space location only depends on the distance from the center of Fourier space. This can be achieved by defining the parameter functions for the prior completely in terms of distance from the origin in Fourier space, i.e., $\pi(\mathcal{F}x_k) = g(|k|)$, and not the orientation with respect to the center of Fourier space. (The "maximally" qualifier is needed because the prior will be isotropic up to the maximal level afforded by the discrete – and anisotropic – specification of Fourier space on a regular, i.e. square, grid.) The relative ease with which isotropy is specified can be contrasted with that of MRF-based priors where local neighborhood characteristics need to be carefully manipulated by increasing neighborhood size and adjusting parameter values to induce approximate spatial isotropy (Rue and Tjelmeland, 2002). For MRFs, pairwise interaction parameters for diagonal neighbors need to be specified differently to horizontal/vertical ones, requiring something of a balancing process to lead to an approximately isotropic process overall. However, for BIFS all that is required to achieve "maximal" isotropy is that the parameter functions are specified such that they only depend on the distance from the origin of Fourier space. Note however, that even for BIFS priors it may still be possible to adjust the parameter function to lead to greater isotropy in practice by tweaking the parameter function to undo anisotropy effects due to Fourier space discretization, though it is not obvious how one might go about achieving this.

Although easy to specify as such, isotropy is clearly not a requirement of the BIFS prior formulation. Anisotropy can be induced by allowing the parameter functions for the prior to vary in different ways with distance from the origin of Fourier space along different directions.

4 Approximating Markov random fields with BIFS

Given that MRF priors have become something of a standard in Bayesian image analysis, it would be useful to generate BIFS models to try and match these commonly used priors. We propose an approach to specifying a prior that is close to an MRF of interest but also potentially "maximally isotropic". The goal is to create BIFS models that are approximate matches, but that have 1) increased computational ease and speed (by specifying as independent over Fourier space locations); 2) increased isotropy if desired (i.e., reduced directional preferences); and 3) resolution invariance.

To find a formulation in Fourier space that approximately matches a corresponding MRF model we propose taking the steps described in Algorithm 2.

Note that it is possible to take this approach when estimating a BIFS approximation to any Bayesian image analysis prior model, though the potential to match higher-level priors (e.g. ones that directly model geometric properties of objects in the image) is likely to be much less of a good approximation.

Algorithm 2 Simulating MRF models with BIFS

- 1: Simulate a set of images from the MRF prior distribution and take the FFT of each image
 - 2: Determine a model for the prior probability distribution of the modulus to be used and independently estimate its' parameters at each Fourier space location
 - 3: Determine an appropriate parameter function form over Fourier space for each of the parameters from the chosen prior based on estimates from the simulated data. (If maximally isotropic approximations to the prior are required then the parameter functions need to be chosen subject to the constraint that it only depends only on distance from the origin of Fourier space)
 - 4: Estimate the coefficients of the parameter function by fitting to the marginally estimated parameters in Fourier space, e.g. via least squares
-

4.1 Example 4 - Matching Gaussian MRFs

We here consider using the above ideas to approximate the simple first-order pairwise difference intrinsic Gaussian MRF (IG-MRF)

$$\pi(x) \propto \exp \left\{ -\frac{\kappa}{2} \sum_{i \sim j} (x_i - x_j)^2 \right\}$$

as described in Besag (1989). The sum over $i \sim j$ is over all unordered pairs of pixels such that i and j are vertically or horizontally adjacent neighbors in the image. The model is called *intrinsic* because the overall mean is not defined and therefore the prior is improper with respect to the overall mean level.

We used the R-INLA package to simulate 1,000 realizations of a first-order IG-MRF with $\kappa = 1.0$ and first-order neighborhood structure wrapped on a torus. At each Fourier space location we adopted a prior distribution for the modulus such that the square of the modulus is distributed as exponential. This choice of prior falls in line with the theoretical results in (Rue and Held, 2005), Ch 2.6 for the specific case of simulating a Gaussian Markov random field with neighborhood structure wrapped on a torus (i.e. with block-circulant precision matrix).

Specifically, an IG-MRF has a precision matrix \mathbf{Q} that is block circulant, in which case we can show using the analysis in (Rue and Held, 2005) that the priors in Fourier space are such that the power at each frequency pair is exponentially distributed. The proof is straightforward but notationally complex so we present the 1 dimensional proof to provide intuition.

The key idea is that if \mathbf{Q} is a circulant matrix then we can decompose it as $\mathbf{Q} = \mathbf{F}\mathbf{\Lambda}\mathbf{F}^H$, where \mathbf{F} is the (discrete) Fourier transform (DFT) matrix, \mathbf{F}^H is the Hermitian (i.e. conjugate transpose of \mathbf{F}), and $\mathbf{\Lambda}$ is a diagonal matrix of eigenvalues of \mathbf{Q} . Now we can compute,

$$\pi(\mathbf{x}) \propto \exp(-\mathbf{x}^T \mathbf{Q} \mathbf{x}) = \exp(-\mathbf{x}^T \mathbf{F} \mathbf{\Lambda} \mathbf{F}^H \mathbf{x}) = \exp(-\mathbf{F}^T \mathbf{x} \mathbf{\Lambda} \mathbf{F}^H \mathbf{x}) = \exp(-\mathbf{F} \mathbf{x} \mathbf{\Lambda} \mathbf{F}^H \mathbf{x})$$

Now let f be the DFT of \mathbf{x} , f^\dagger the inverse DFT (IDFT) of \mathbf{x} , and p_k the power at frequency k , so

$$\pi(\mathbf{x}) \propto \exp(-f \mathbf{\Lambda} f^\dagger) = \exp\left(\sum_k -\lambda_k f_k f_k^\dagger\right) = \exp\left(\sum_k -\lambda_k p_k\right) = \prod_k \exp(-\lambda_k p_k)$$

This final term is a product of functions so the distributions at each frequency are independent and each has an exponential distribution.

$$\pi(p, \theta) \propto \prod_k \exp(-\lambda_k p_k).$$

To summarize, this shows that for GMRFs with neighborhood structure specified on the torus, the power spectrum (the square of the signal modulus) is made up of independent exponential random variables.

We need to obtain the posterior maximum for the prior where the modulus square follows an exponential distribution coupled with Rician noise, analogous to that of Equation 7 for when the exponential prior was used directly for the modulus.

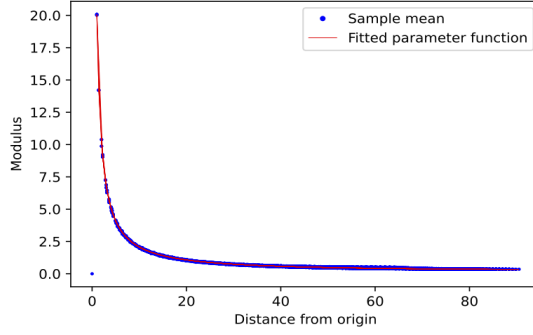


Figure 6: Parameter model fit for modulus as a function of distance from the origin of Fourier space

Assume that $X \sim \text{Exp}(1/m)$ for each point in Fourier space and that $P = \sqrt{X}$. Then for any $\rho \geq 0$;

$$\Pr(P \leq \rho) = \Pr(\sqrt{X} \leq \rho) = \Pr(X \leq \rho^2) = 1 - \exp\left(-\frac{\rho^2}{m}\right) \quad \rho \geq 0$$

differentiating, we get the pdf for the prior of ρ :

$$\pi(\rho|m) = \frac{2\rho}{m} \exp\left(-\frac{\rho^2}{m}\right) \quad \rho \geq 0$$

now applying Bayes' Theorem and taking logs to simplify

$$\log \pi(\rho|r, \sigma, m) = c - \frac{\rho^2}{2\sigma^2} + \log\left(I_0\left(\frac{r\rho}{\sigma^2}\right)\right) + \log\left(\frac{2\rho}{m}\right) - \frac{\rho^2}{m}$$

differentiate w.r.t. ρ

$$\frac{d \log \pi(\rho|r, \sigma, m)}{d\rho} = -\frac{\rho}{\sigma^2} + \frac{r I_1\left(\frac{r\rho}{\sigma^2}\right)}{\sigma^2 I_0\left(\frac{r\rho}{\sigma^2}\right)} + \frac{1}{\rho} - \frac{2\rho}{m}$$

then set equal to zero and solve to get the positive solution for ρ of

$$\rho = \frac{rmb(\rho) + \sqrt{(b(\rho)rm)^2 + 8\sigma^4m + 4(\sigma m)^2}}{4\sigma^2 + 2m}. \quad (8)$$

However, instead of exactly matching the MRF using the eigenvalues to model the IG-MRF in Fourier space as in (Rue and Held, 2005), we instead fit an isotropic parameter function to the mean of the modulus at each Fourier space location using least squares. The form of the parameter function used was

$$f(|k|; \mathbf{a}) = \frac{a_0}{a_1 + a_2|k| + a_3|k|^2 + a_4|k|^3}$$

(chosen based on a trial-and-error approach to get a good least squares fit – See Figure 6).

Simulations from the BIFS prior were well-matched to their MRF counterpart. Figure 7 shows example realizations from each of the BIFS and direct MRF simulations in panels (a) and (b) respectively and they clearly exhibit similar properties. Panel (c) shows the respective estimated autocovariance functions (ACFs) as a function of distance from 1,000 simulations of each random field. The spread observed in the estimated ACFs at longer distances is due to the anisotropy of the processes induced by the rectangular lattice and for the MRF because of the anisotropic representation of the neighborhood structure; hence the slightly narrower band for the BIFS simulations (see Section 3.3).

In order to compare posterior estimates between the two approaches we examine a simulated dataset generated using a version of the Montreal Neurological Institute (MNI) brain (Cocosco et al.) that had been

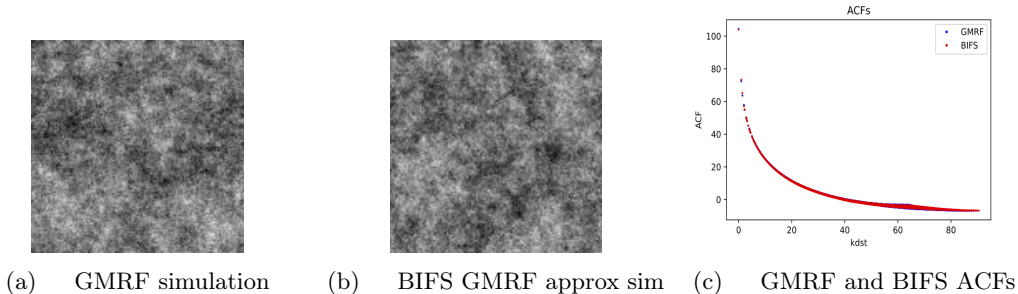


Figure 7: Example simulations for the first order intrinsic GMRF using a direct approach in R-INLA in panel (a) and the BIFS approximation with isotropic parameter function in panel (b). The estimated ACF as a function of distance for each of the simulated models is given in panel (c).

segmented into gray matter (GM), white matter (WM), and cerebro-spinal fluid (CSF)/outside brain at 128 by 128 resolution. GM is the outer ribbon (the cortex) around the brain where neuronal activity occurs, WM is made up of the connective strands that enable different regions of the cortex to communicate with each other, and CSF is fluid in the brain. The signal was generated with intensity 20.0 in GM, 10.0 in WM and 0.0 elsewhere and is displayed in Panel (a) of Figure 8. Gaussian noise (*i.i.d.*) with SD of 2.5 was added to generate a degraded image as displayed in Panel (b).

The image was reconstructed as a MAP estimate from the degraded data using each of the IG-MRF prior (with conjugate gradients optimization) and BIFS “maximally isotropic” equivalent prior approximation. Comparing the IG-MRF and corresponding BIFS reconstructions in Panels (c) and (d), respectively, indicates that the MRF and BIFS are indistinguishable visually. This is confirmed when looking at the residual maps in panels (e) and (f) which are also indistinguishable. Note that Panels (a) to (d) are normalized to be on the same dynamic scale (i.e. such that the same value corresponds to each gray-scale shade). Similarly, Panels (e) and (f) are matched to a dynamic scale over the range of the residuals in both images. Of note is that the residuals for both MRFs and BIFS carry considerable residual structure. This is simply a reflection of the nature of the priors in only representing local characteristics as discussed in Section 2.7

The level of similarity between the two reconstructions is further emphasized in Table 1. The table gives a comparison of mean signal estimates in each tissue type along with overall predictive accuracy based on root-mean-square-error (RMSE) over all pixels in the image. The results are very similar comparing IG-MRF and BIFS, indicating that BIFS is doing a good job of approximating the results of IG-MRF. Both models shrink estimates of mean tissue levels toward neighboring tissue types due to the overall smoothing effect of the Gaussian pairwise difference prior. This bias effect is largest in GM where the tissue region is narrow and therefore the conditional distributions within GM regions often include neighbors from other tissue types, which for GM will lead to biasing down the pixel estimates. In fact, this smoothing bias is strong enough to increase the RMSE for the Bayesian reconstructions compared with just using the noisy data. This emphasizes the dangers of blindly using Bayesian image analysis when the goal is estimation.

The results are very slightly better for BIFS than ICM-GMRF in terms of having slightly smaller differences from the true values, though one needs to be careful not to over-interpret this very small difference. The different results are simply due to using slightly different models and one could easily find datasets or/and models that fit better with respect to RMSE in either the MRF or BIFS frameworks. However, it should be noted again, that as mentioned in Section 3.1 it is much easier to try different models in the BIFS framework e.g. via simply changing the form of the parameter function than it is to try different MRF priors.

5 The data-driven BIFS Prior (DD-BIFS)

The standard process of generating the BIFS prior distribution described in Section 2.1 is based on choosing a pair of distributions to be applied as priors at each location in Fourier space (one for the modulus and the other for the argument of the complex value signal) and a set of parameter functions to define how the parameters of the distributions vary over Fourier space. In contrast, for the data-driven approach the

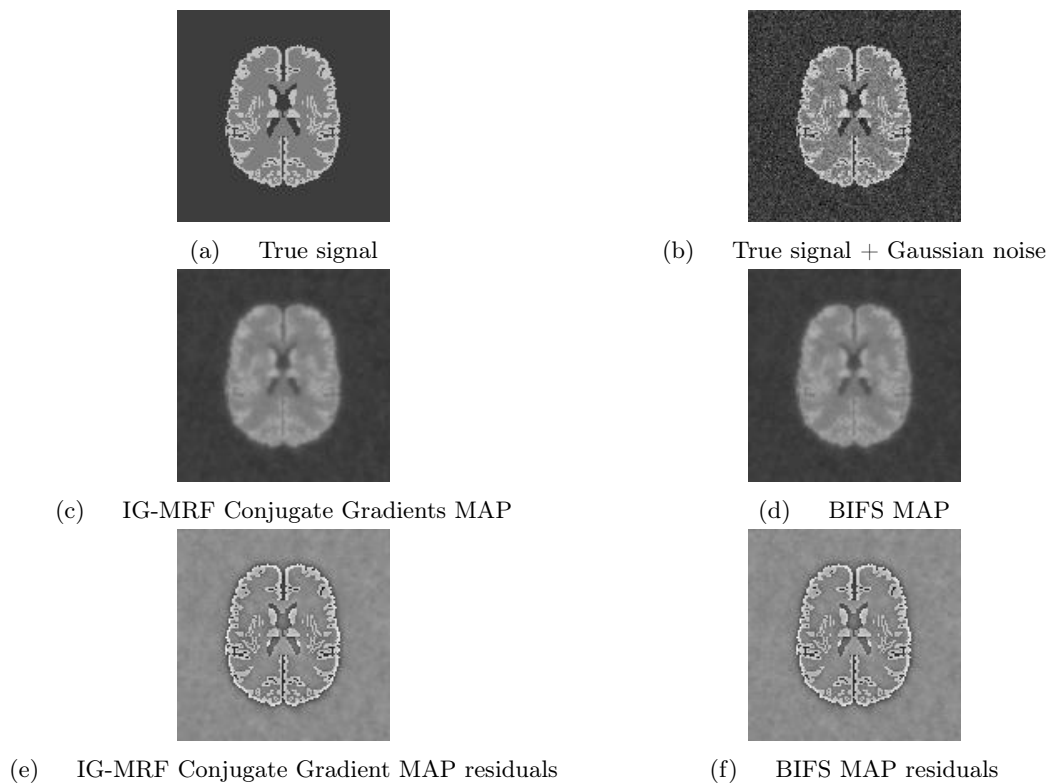


Figure 8: BIFS match to IG-MRF prior for perfusion MRI simulation study. (a) simulated brain signal image; (b) image of the same data with added Gaussian noise (c) IG-MRF MAP reconstruction from the noisy data (using conjugate gradients optimization); (d) BIFS MAP reconstruction based on maximally isotropic approximation to IG-MRF; (e) IG-MRF MAP residuals (relative to true signal of Panel (a)); (f) BIFS MAP residuals. Panels (a) to (d) are normalized to be on the same dynamic scale. Similarly, Panels (e) and (f) are matched to a dynamic scale over the range of the residuals in both images.

Table 1: Comparison between estimates of mean signal in each tissue type and overall RMSE of reconstructions.

	True	True + noise	IG-MRF	BIFS
GM	20.0	19.92	13.48	13.53
WM	10.0	9.99	11.10	11.08
CSF/out	0.0	-0.01	0.54	0.54
RMSE	0.0	2.47	2.74	2.71

parameters at each Fourier space location are estimated empirically from a database of transformed images. The database of images would be of high-quality and have the characteristics that are required to represent the prior specification.

To estimate the parameters, all of the images in the database are first Fourier transformed, the data at each location in Fourier space are extracted (i.e. for all images), and the distribution parameters for that Fourier space location are estimated from that data. These parameter estimates are then used to define the parameters for the prior at each Fourier space location, i.e. they form the basis of the parameter functions. (Note that when the database is not large it may be more beneficial to fit parameter functions to the empirical data rather than use estimates generated separately at each Fourier space location.)

The implementation of DD-BIFS modeling follows the steps of Algorithm 3.

Algorithm 3 DD-BIFS modeling

- 1: Fast Fourier transform (FFT) all images in the database that are to be used to build the DD-BIFS prior
 - 2: Choose the distributional form of the prior at each location in Fourier space
 - 3: Estimate the parameters of the prior at each location in Fourier space using the data from that Fourier space location across the subjects in the database
 - 4: Scale the sets of parameters over Fourier space to adjust the influence of the prior – this is the DD-BIFS prior
 - 5: Define the likelihood in Fourier space
 - 6: FFT the dataset to be reconstructed from image space into Fourier space
 - 7: Combine the DD-BIFS prior and likelihood for the image at each Fourier space location via Bayes’ Theorem to generate the DD-BIFS posterior
 - 8: Generate the Fourier space MAP estimate by maximizing the posterior at each Fourier space location
 - 9: Inverse FFT the Fourier space MAP estimate back to image space and display
-

5.1 Example 5 - Data-driven prior simulation study

To illustrate the DD-BIFS approach we simulated 10,000 256×256 images containing ellipsoid objects. The number of objects was modeled as a Poisson process; the objects were simulated as randomly positioned 2D Gaussian probability density functions (resembling bumps) with random intensity, and standard deviation on each axis, and correlation between the standard deviations on each axis distributed uniformly between -1 and 0, i.e., so that the process was not isotropic.

We generated an additional realization (separate to the 10,000 used to build the prior) displayed in Figure 9a and contaminated it with added Gaussian noise (Figure 9b). We then performed DD-BIFS with MAP estimation for this single new realization from the process.

For this reconstruction we used a deliberately miss-specified prior and likelihood below to allow a simple illustration using conjugate prior forms. At each Fourier space location k we adopt a truncated Gaussian prior for the modulus: $\text{Mod}(\mathcal{F}x_k) \sim TN(\mu_k, \tau_k^2, 0, \infty)$, with $\mu_k \geq 0$; a Uniform prior on the circle for the argument: $\text{Arg}(\mathcal{F}x_k) \sim U(0, 2\pi)$, a Gaussian noise model for the modulus $\text{Mod}(\epsilon_k) \sim N(0, \sigma^2)$, and a Uniform noise model for the argument $\text{Arg}(\epsilon_k) \sim U(0, 2\pi)$, where ϵ_k is the complex noise treated as independent across Fourier space locations k . (Note this model does not correspond to the simulated Gaussian noise in image space, which would require the Rician likelihood used previously.) The values of μ_k and σ_k at each Fourier

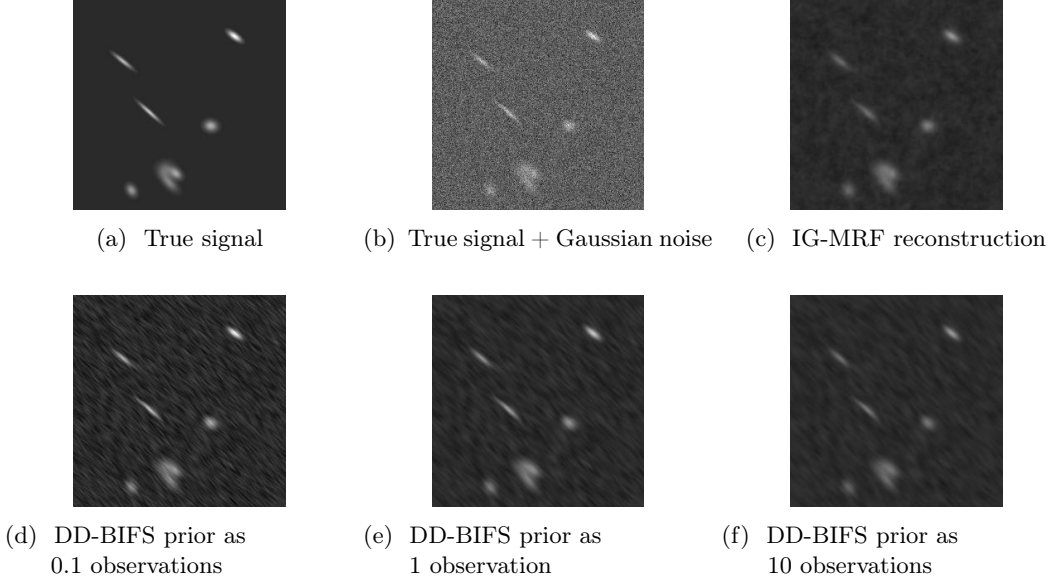


Figure 9: Simulation study and reconstruction of anisotropic bump patterns. Panel (a) new process realization; (b) realization with added noise; (c) first order IG-MRF reconstruction; (d) DD-BIFS prior equivalent to 0.1 observations (e) DD-BIFS prior 1 observation; (f) DD-BIFS for 10 observations. All panels except for Panel (b) are normalized to be on the same dynamic scale.

space location are estimated using the approach outlined in Algorithm 3.

The global posterior mode is then obtained by generating the posterior mean based on conjugate Bayes for the corresponding non-truncated Gaussian prior and likelihood, which is equivalent to the posterior mode and hence the posterior mode of the truncated prior version, at each Fourier space location (Gelman et al., 2014) with

$$x_{k,\text{MAP}} = \frac{\left(\frac{m\mu_k}{\tau_k^2} + \frac{y_k}{\sigma^2}\right)}{\left(\frac{m}{\tau_k^2} + \frac{1}{\sigma^2}\right)}$$

Note that the value of m in the prior is specified by the user and can be considered to represent how many observations we want the weight of the prior to count for in the posterior.

Panel (c) of Figure 9 shows an IG-MRF reconstruction of the noisy data. It clearly denoises the image but at the expense of smoothing the objects in the image. Panels (d) through (f) shows the a DD-BIFS reconstruction where the database prior is given weight equivalent to 0.1, 1.0 and 10.0 observations respectively. Note that in general for these priors the bumps that are elongated have their length better preserved than in the Gaussian prior case. As the number of observations that the DD-BIFS prior represents increases the features of the true signal begin to diminish and the noise level of the reconstruction is reduced. This makes sense because in the limit we would effectively be obtaining the MAP estimate based on the prior alone which is an average over 10,000 simulations. Note that this high-level capturing of the bump features occurs despite the independence specification in Fourier space; the BIFS formulation is able to capture the anisotropic characteristics of these features through the empirical parameter function. Note also that the DD-BIFS prior could itself be modified by changing the form of the parameter function. For example, if one wanted to diminish the anisotropic features of the background signal the prior could be taken as a function of both the database prior and a denoising parameter function.

6 Discussion and Conclusion

The BIFS modeling framework provides a new family of Bayesian image analysis models with the capacity to a) enhance images beyond conventional standard Bayesian image analysis methods; b) allow straightforward specification and implementation across a wide range of imaging research applications; and c) enable fast and high-throughput processing. These benefits, along with the inherent properties of resolution invariance and isotropy, make BIFS a powerful tool for the image analysis practitioner.

A particular strength of the BIFS approach is the ease with which one is able to try different prior models. Experimenting with different priors might be considered problematic in other fields, but in Bayesian image analysis we typically know in advance that any model we can specify will be wrong and at best can approximately capture some characteristics from the image; if we simulate from Bayesian image analysis priors we would expect to be waiting an extremely long time before we see a realization that would be representative of an object of interest (e.g. a brain or a car). It is therefore often of benefit to try different models until finding a prior that has the desired impact on the posterior. This approach would have additional legitimacy if one reserves images purely for the purpose of formulating a preferred prior before analyzing the images of interest.

The BIFS framework has much potential for future work to expand the foundations presented here: BIFS could be applied to spatio-temporal modeling, multi-image analysis, multi-modal medical imaging, color images, 3D images, other spatial basis spaces such as wavelets, multifractal modeling, non-continuous valued MRFs with hidden latent models, etc. We hope that other statisticians, engineers, and computer scientists with an interest in image analysis will begin to explore these potential areas.

Acknowledgements

Research reported in this manuscript was supported by National Institute of Biomedical Imaging and Bioengineering of the National Institutes of Health under award number R01EB022055.

Thanks to Hernando Ombao, Hävard Rue, Konstantinos Bakas, William Braithwaite and Rui Zhang for comments on manuscript; Chuck McCulloch, John Neuhaus, and Saunak Sen for general advice; Ross Boylan for Python package programming.

Code

All code used in this manuscript is available at: <https://github.com/ucsf-deb/BIFSpaper1>

References

- Abramovich, F., Sapatinas, T. and Silverman, B. W. (1998) Wavelet thresholding via a bayesian approach. *Journal of the Royal Statistical Society: Series B (Statistical Methodology)*, **60**, 725–749.
- Baddeley, A. J. and van Lieshout, M. N. M. (1993) Stochastic geometry models in high-level vision. *Journal of Applied Statistics*, **20**, 231–256.
- Baskaran, S. and Millane, R. P. (1999) Bayesian image reconstruction from partial image and aliased spectral intensity data. *Image Processing, IEEE Transactions on*, **8**, 1420–1434.
- Besag, J. (1974) Spatial interaction and the statistical analysis of lattice systems (with discussion). *Journal of the Royal Statistical Society. Series B (Methodological)*, **36**, 192–236.
- (1986) On the statistical analysis of dirty pictures (with discussion). *Journal of the Royal Statistical Society. Series B (Methodological)*, **48**, 259–302.
- (1989) Digital image processing: Towards bayesian image analysis. *Journal of Applied statistics*, **16**, 395–407.
- (1993) Towards Bayesian image analysis. *Journal of Applied statistics*, **20**, 107–109.

- Besag, J. E., York, J. and Mollié, A. (1991) Bayesian image restoration with two applications in spatial statistics (with discussion). *Ann. Inst. Statist. Math.*, **43**, 1–59.
- Buccigrossi, R. W. and Simoncelli, E. P. (1999) Image compression via joint statistical characterization in the wavelet domain. *Image Processing, IEEE Transactions on*, **8**, 1688–1701.
- Candès, E. and Donoho, D. (2004) New tight frames of curvelets and optimal representations of objects with piecewise c_2 singularities. *Communications on pure and applied mathematics*, **57**, 219–266.
- Chang, S., Yu, B. and Vetterli, M. (2000) Adaptive wavelet thresholding for image denoising and compression. *Image Processing, IEEE Transactions on*, **9**, 1532–1546.
- Chipman, H. A., Kolaczyk, E. D. and McCulloch, R. E. (1997) Adaptive bayesian wavelet shrinkage. *Journal of the American Statistical Association*, **92**, 1413–1421.
- Christmas, J. (2014) Bayesian spectral analysis with student-t noise. *Signal Processing, IEEE Transactions on*, **62**, 2871–2878.
- Cocosco, B., Kollokian, V., Kwan, R. and Evans, A. () online interface to a 3d mri simulated brain database. *NeuroImage*, **5**.
- Donoho, D. L. and Huo, X. (1999) Combined image representation using edgelets and wavelets. In *SPIE's International Symposium on Optical Science, Engineering, and Instrumentation*, 468–476. International Society for Optics and Photonics.
- (2002) *Beamlets and multiscale image analysis*. Springer.
- Figueiredo, M. A. T. and Nowak, R. D. (1999) Bayesian wavelet-based image estimation using noninformative priors. In *SPIE's International Symposium on Optical Science, Engineering, and Instrumentation*, 97–108. International Society for Optics and Photonics.
- Gelman, A., Carlin, J. B., Stern, H. S., Dunson, D. B., Vehtari, A. and Rubin, D. B. (2014) *Bayesian data analysis*, vol. 2. CRC press Boca Raton, FL.
- Geman, S. and Geman, D. (1984) Stochastic relaxation, Gibbs distributions, and the Bayesian restoration of images. *IEEE Transactions on Pattern Analysis and Machine Intelligence*, **6**, 721–741.
- Gilks, W. R., Richardson, S. and Spiegelhalter, D. (1996) *Markov chain Monte Carlo in practice*. Chapman & Hall.
- Green, P. J. (1990) Bayesian reconstructions from emission tomography data using a modified em algorithm. *IEEE transactions on medical imaging*, **9**, 84–93.
- Grenander, U. (1993) *General pattern theory: A mathematical study of regular structures*. Clarendon Press.
- Grenander, U., Srivastava, A. and Miller, M. I. (2000) Asymptotic performance analysis of Bayesian target recognition. *IEEE Transactions on Information Theory*, **46**, 1658–1665.
- Gudbjartsson, H. and Patz, S. (1995) The rician distribution of noisy mri data. *Magnetic resonance in medicine*, **34**, 910–914.
- Guyon, X. (1995) *Random fields on a network: modeling, statistics, and applications*. Springer Science & Business Media.
- Hestenes, M. R. (1969) Multiplier and gradient methods. *Journal of optimization theory and applications*, **4**, 303–320.
- Johnstone, I. M. and Silverman, B. W. (2005) Empirical bayes selection of wavelet thresholds. *Annals of Statistics*, 1700–1752.
- Künsch, H. R. (1987) Intrinsic autoregressions and related models on the two-dimensional lattice. *Biometrika*, **74**, 517–524.

- Lange, N. and Zeger, S. L. (1997) Non-linear fourier time series analysis for human brain mapping by functional magnetic resonance imaging. *Journal of the Royal Statistical Society: Series C (Applied Statistics)*, **46**, 1–29.
- Leporini, D. and Pesquet, J.-C. (2001) Bayesian wavelet denoising: Besov priors and non-gaussian noises. *Signal processing*, **81**, 55–67.
- Levin, A., Fergus, R., Durand, F. and Freeman, W. T. (2007) Image and depth from a conventional camera with a coded aperture. In *ACM Transactions on Graphics (TOG)*, vol. 26;3, 70. ACM.
- Levin, A. and Weiss, Y. (2007) User assisted separation of reflections from a single image using a sparsity prior. *IEEE Transactions on Pattern Analysis & Machine Intelligence*, **29**, 1647–1654.
- Li, M. and Ghosal, S. (2014) Bayesian multiscale smoothing of gaussian noised images. *Bayesian Analysis*, **9**, 733–758.
- Li, S. Z. (2009) *Markov random field modeling in image analysis*. Springer Science & Business Media.
- Liang, Z.-P. and Lauterbur, P. C. (2000) *Principles of magnetic resonance imaging: a signal processing perspective*. SPIE Optical Engineering Press.
- Miolane, N., Holmes, S. and Pennec, X. (2017) Template shape estimation: correcting an asymptotic bias. *SIAM Journal on Imaging Sciences*, **10**, 808–844.
- Morris, J. S. (2014) Functional regression. *arXiv preprint arXiv:1406.4068*.
- Nadarajah, S. and Kotz, S. (2007) The bkf bayesian wavelet estimator. *Signal Processing*, **87**, 2268–2271.
- Olshausen, B. A. (1996) Emergence of simple-cell receptive field properties by learning a sparse code for natural images. *Nature*, **381**, 607–609.
- Pavlicová, M., Santner, T. J. and Cressie, N. (2008) Detecting signals in fmri data using powerful fdr procedures. *Statistics and Its Interface*, **1**, 23–32.
- Peligrad, M. and Utev, S. (2006) Central limit theorem for stationary linear processes. *The Annals of Probability*, **34**, 1608–1622.
- Portilla, J., Strela, V., Wainwright, M. J. and Simoncelli, E. P. (2003) Image denoising using scale mixtures of gaussians in the wavelet domain. *Image Processing, IEEE Transactions on*, **12**, 1338–1351.
- Ramsay, J. O. and Silverman, B. W. (2002) *Applied functional data analysis: methods and case studies*, vol. 77. Citeseer.
- (2005) *Functional Data Analysis*. Springer.
- Ray, S. and Mallick, B. (2006) Functional clustering by bayesian wavelet methods. *Journal of the Royal Statistical Society: Series B (Statistical Methodology)*, **68**, 305–332.
- Rice, S. O. (1944) Mathematical analysis of random noise. *Bell Labs Technical Journal*, **23**, 282–332.
- (1945) Mathematical analysis of random noise. *The Bell System Technical Journal*, **24**, 46–156.
- Ritter, G. and Gallegos, M. T. (2002) Bayesian object identification: variants. *Journal of Multivariate Analysis*, **81**, 301–334.
- Rowe, D. B. and Logan, B. R. (2004) A complex way to compute fmri activation. *Neuroimage*, **23**, 1078–1092.
- Rue, H. and Held, L. (2005) *Gaussian Markov random fields: theory and applications*. CRC press.
- Rue, H. and Hurn, M. A. (1999) Bayesian object identification. *Biometrika*, **86**, 649–660.

- Rue, H. and Tjelmeland, H. (2002) Fitting gaussian markov random fields to gaussian fields. *Scandinavian journal of Statistics*, **29**, 31–49.
- Sheikh, Y. and Shah, M. (2005) Bayesian object detection in dynamic scenes. In *Computer Vision and Pattern Recognition, 2005. CVPR 2005. IEEE Computer Society Conference on*, vol. 1, 74–79. IEEE.
- Sonka, M., Hlavac, V. and Boyle, R. (2014) *Image processing, analysis, and machine vision*. Cengage Learning.
- Sørbye, S. H. and Rue, H. (2014) Scaling intrinsic gaussian markov random field priors in spatial modelling. *Spatial Statistics*, **8**, 39–51.
- Staib, L. H. and Duncan, J. S. (1992) Boundary finding with parametrically deformable models. *IEEE Transactions on Pattern Analysis & Machine Intelligence*, 1061–1075.
- Swain, M. J., Wixson, L. E. and Chou, P. B. (2013) Efficient parallel estimation for markov random fields. *arXiv preprint arXiv:1304.1532*.
- Vijay, M., Devi, L., Shankaravadivu, M. and Santhanamari, M. (2012) Image denoising based on adaptive spatial and wavelet thresholding methods. In *Advances in Engineering, Science and Management (ICAESM), 2012 International Conference on*, 161–166. IEEE.
- Winkler, G. (1995) *Image analysis, random fields and dynamic Monte Carlo methods: A Mathematical Introduction*. Springer.
- Zeger, S. L. (1985) Exploring an ozone spatial time series in the frequency domain. *Journal of the American Statistical Association*, **80**, 323–331.